Visible-Light Acceleration of H 2 Evolution from Aqueous Solutions of Inorganic Hydrides Catalyzed by Gold-Transition-Metal Nanoalloys

Naixin Kang, Qi Wang, Rodrigue Djeda, Wenjuan Wang, Fangyu Fu, Marta Martinez Moro, Maria de Los Angeles Ramirez, Sergio Moya, Emerson Coy, L. Salmon, et al.

▶ **To cite this version:**

Naixin Kang, Qi Wang, Rodrigue Djeda, Wenjuan Wang, Fangyu Fu, et al.. Visible-Light Acceleration of H 2 Evolution from Aqueous Solutions of Inorganic Hydrides Catalyzed by Gold-Transition-Metal Nanoalloys. ACS Applied Materials & Interfaces, 2020, 12 (48), pp.53816-53826. 10.1021/acsami.0c16247 . hal-03225580

HAL Id: hal-03225580
https://hal.science/hal-03225580

Submitted on 17 May 2021

HAL is a multi-disciplinary open access archive for the deposit and dissemination of scientific research documents, whether they are published or not. The documents may come from teaching and research institutions in France or abroad, or from public or private research centers.

L'archive ouverte pluridisciplinaire **HAL**, est destinée au dépôt et à la diffusion de documents scientifiques de niveau recherche, publiés ou non, émanant des établissements d'enseignement et de recherche français ou étrangers, des laboratoires publics ou privés.

Visible-light Acceleration of H_2 Evolution from Aqueous Solutions of Inorganic Hydrides Catalyzed by Gold-Transition-Metal Nanoalloys

*Naixin Kang,[a] Qi Wang,[a] Rodrigue Djeda,[a] Wenjuan Wang,[a] Fangyu Fu,[a] Marta Martinez Moro,[b] Maria de los Angeles Ramirez,[b,c] Sergio Moya,[b,d] Emerson Coy,[d] Lionel Salmon,[e] Jean-Luc Pozzo,[a] Didier Astruc[a,]**

[a]ISM, UMR CNRS N° 5255, Univ. Bordeaux, 33405 Talence Cedex, France.

[b]Soft Matter Nanotechnology Lab, CIC biomaGUNE, Paseo Miramón 182. 20014. Donostia-San Sebastián, Gipuzkoa, Spain.

[c]Instituto de Nanosistemas (Unsam, Coniset), Av. 25 de mayo 1021, 1650 San Martin, Buenos Aeres, Argentina

[d]NanoBioMedical Centre, Adam Mickiewicz University in Poznań, Wszechnicy Piastowskiej 3, 61-614 Poznań, Poland.

[e]LCC, CNRS & University of Toulouse III, 205 Route de Narbonne, 31077 Toulouse Cedex, France.

ABSTRACT

Production of hydrogen (H_2) upon hydrolysis of inorganic hydrides potentially is a key step in green energy production. We find that visible-light irradiation of aqueous solutions of ammonia-borane (AB) or $NaBH_4$ containing "click"-dendrimer-stabilized alloyed nanocatalysts composed of nanogold and another late transition-metal nanoparticle (LTMNP) highly enhances catalytic activity for H_2 generation while also inducing alloy to Au core@M shell nanocatalyst restructuration. In terms of visible-light-induced acceleration of H_2 production from both AB and $NaBH_4$, the Au_1Ru_1 alloy catalysts show the most significant light boosting effect. Au-Rh and Au-PtNPs are also remarkable with total H_2 release time from AB and $NaBH_4$ down to 1.3 min at 25 °C (AuRh), three times less than in the dark, and Co is the best earth-abundant metal alloyed with nanogold. This boosting effect is explained by the transfer of plasmon-induced hot electron from the Au atoms to the LTMNP atoms facilitating water O-H oxidative addition on the LTMNP surface, as shown by the large primary kinetic isotope effect k_H/k_D upon using D_2O obtained for both AB and $NaBH_4$. The second simultaneous and progressive effect of visible-light irradiation during these reactions, alloy to Au core@M shell restructuration, enhances the catalytic activity in the recycling, because, in the resulting Au core@M shell, the surface metal (such as Ru) is much more active that the original Au-containing alloy surface in dark reactions. There is no light effect on the rate of hydrogen production for the recycled nanocatalyst due to the absence of Au on the NP surface, but it is still very efficient in hydrogen release during 4 cycles, due to the initial light-induced restructuration, although it is slightly less efficient than the original nanoalloy in the presence of light. The dendritic triazole coordination on each LTMNP surface appears to play a key role in these remarkable light-induced processes.

KEYWORDS: Plasmon, hydrogen production, bimetallic nanoparticles, nanogold, boron hydride

INTRODUCTION

Production of hydrogen (H_2) from non-fossil sources has become a priority in the 21st century's research. [1, 2] Since the seminal work of Fujushima and Honda in 1972,[3] solar-light irradiation for water splitting using electron/hole pair formation of semiconductor catalysts has long been considered as an attractive solution, although it finds some practical limits concerning the nanoengineering of the materials involved.[4-8] Recently, hot electrons generated in the 1-100 fs range by visible light irradiation of gold plasmon are also promising for transfer of such electrons to an adjacent semiconductor conduction band.[9] In practice, however, the mismatch between the short lifetimes of hot electrons and the slow kinetics of reactions at the semiconductor surface has been a major limitation to the efficiencies of these plasmonic photocatalyzed reactions.[10, 11] Semiconductors may most of the time also be toxic and of modest efficiency, and alternative solutions are continuously searched. Visible-light acceleration of a number of various catalytic reactions of synthetic and environmental interest has been reported for plasmonic gold as part of heterobimetallic catalysts.[12] In particular, interest has recently focused on plasmon induced light acceleration of hydrolysis of ammonia-borane (AB), NH_3BH_3, by coinage metal NPs using heterobimetallic nanocatalysts either coupled to[13-18] or without a semi-conductor.[19-23] Inorganic hydrides such as AB and sodium borohydride, $NaBH_4$, are promising hydrogen storage compounds,[24-26] because they are stable solids with high colloidal solubility in water, contain a high proportion of hydrogen and are easily transported contrary to explosive hydrogen gas.[27, 28] Also, AB is inert toward hydrolysis, and $NaBH_4$ is hydrolyzed only very slowly in the absence of catalyst.[29] Therefore, research efforts have recently been devoted to the optimization of catalysts for H_2 generation from water and such inorganic hydrides.[30-36] Heterobimetallic NP catalysts have attracted much attention because of the possible synergies between the two metals forming the NP.[37-47] Concerning photocatalytic AB dehydrogenation, Li's group reported theoretical calculations showing the presence of a special plasmonic resonance mode at the interphase of bimetallic core-shell NPs, adding to the surface mode.[48] The Yamashita group reported enhanced catalytic activity of small SBA-15 stabilized AgNPs upon visible-light irradiation for H_2

generation from AB hydrolysis without any other metal catalyst.[49] The same group reported an enhancement factor of 2.8 upon visible-light irradiation of SBA-15-supported Pt-Ag NPs.[13] Huang's group reported the facet-dependent light-assisted hydrogen generation from AB using large (32 nm) Au-Pd core-shell nanocatalysts.[20] Previous studies from our group on hydrogen evolution from AB in the dark have dealt with group 9 and 10 metal nanocatalysts,[30, 32, 50] and positive synergistic effects have been disclosed with Co-Pt [50] and Ni-Pt NPs.[32] AuNPs benefit from an enhanced kinetic stability under aerobic conditions and have attracted an enormous amount of interest in various fields including biomedicine, optics and catalysis.[51]

We report here the acceleration effects of visible-light irradiation on the catalytic activity of a series of bimetallic Au-late transition metal NPs (LTMNPs) for H_2 production upon reaction of water with the boron hydrides AB and $NaBH_4$. During these same reactions, a second light effect observed is the progressive restructuration in several cases of the alloy nanocatalysts to core-shell Au@M. Comparison is made with monometallic LTMNP nanocatalysts that, as nanogold, are not subjected to any light effect under the same conditions. Indeed, remarkable boosting effects of visible light are disclosed here with bimetallic nanogold-containing alloyed nanocatalysts supported by "click" dendrimers or a "click" polymer.

RESULTS AND DISCUSSION

Macromolecule-stabilized nanocatalysts

The known water-soluble "click" dendrimers **1** (with an approximate diameter size of 10 nm) and **2** (with an approximate diameter size of 15 nm)[52] (Scheme 1) are catalyst templates acting as unimolecular micelles.[53] They stabilize molecular, cationic and LTMNP catalysts with small size leading to excellent catalytic results due to confinement of the catalyst and substrates in the dendritic interior including tris-triazole-containing tripods. The known "click" polymer **3**[53] (Scheme 1 and S2) and poly(vinylpyrrolidone) (PVP) were also used as supports for comparison. Upon mixing the metal salt precursor and the dendrimer **1** or **2** or polymer **3** in water, a H_2O ligand of the metal cation is exchanged by the triazole ligand; thus, the metal cation keeps the same positive charge. In the case of the Pd and Pt tetrachlorometallates, an anionic chloride ligand of the square-planar complex MCl_4^{2-} is replaced by a neutral triazole ligand. Formally, the charge of the metal complex then changes from -2 to -1, whereas the metal oxidation state (II) remains unchanged (Scheme S3). Upon reduction of all these macromolecule-coordinated metal derivatives by $NaBH_4$, the oxidation state of all the metals is decreased to zero, and the atoms collapse into a LTMNP catalyst loosely stabilized by both the heteroatoms and bulk of the macromolecule. When 1 mmol AB (or $NaBH_4$) is completely hydrolyzed upon catalysis by the "click"-dendrimer-stabilized LTMNP, 3 (or 4) mmol of H_2 (67 or 89 mL) are produced, indicating reaction completion, in equations (1) or (2), respectively. In both reactions, a metaborate salt is formed in a di-hydrated form MBO_2, $2H_2O$, i.e. $MB(OH)_4$, M = Na or NH_4, and reaction intermediates were not detected.

$$NH_3BH_3 + 4H_2O \rightarrow NH_4^+B(OH)_4^- + 3H_2 \quad (1)$$

$$NaBH_4 + 4H_2O \rightarrow NaB(OH)_4 + 4H_2 \quad (2)$$

Most studies have been conducted using the click dendrimer **1** and, unless noted otherwise, results are reported in text with dendrimer **1**. In order to compare the above catalyzed reactions under dark and visible-light conditions, first, click-dendrimer-stabilized monometallic LTMNPs have been synthesized

(Scheme 1), as previously reported,[50] by reduction of the click-dendrimer-coordinated M(II) or M(III) species to M(0) using $NaBH_4$. The other LTMNPs were found to be better catalysts than AuNPs (a poor catalyst in this reaction) and, in all these cases, no catalytic enhancement was found upon visible-light irradiation, even with the monometallic AuNPs (Table 1). Then, click-dendrimer stabilized bimetallic Au-M NPs (M = Ni, Co, Ru, Rh, Pd, Pt or Ag) were synthesized by pre-coordination of both Au(III) and M(II) species to intra-dendritic triazole ligands followed by reduction of both M(II) and Au(III) to M(0) using $NaBH_4$.

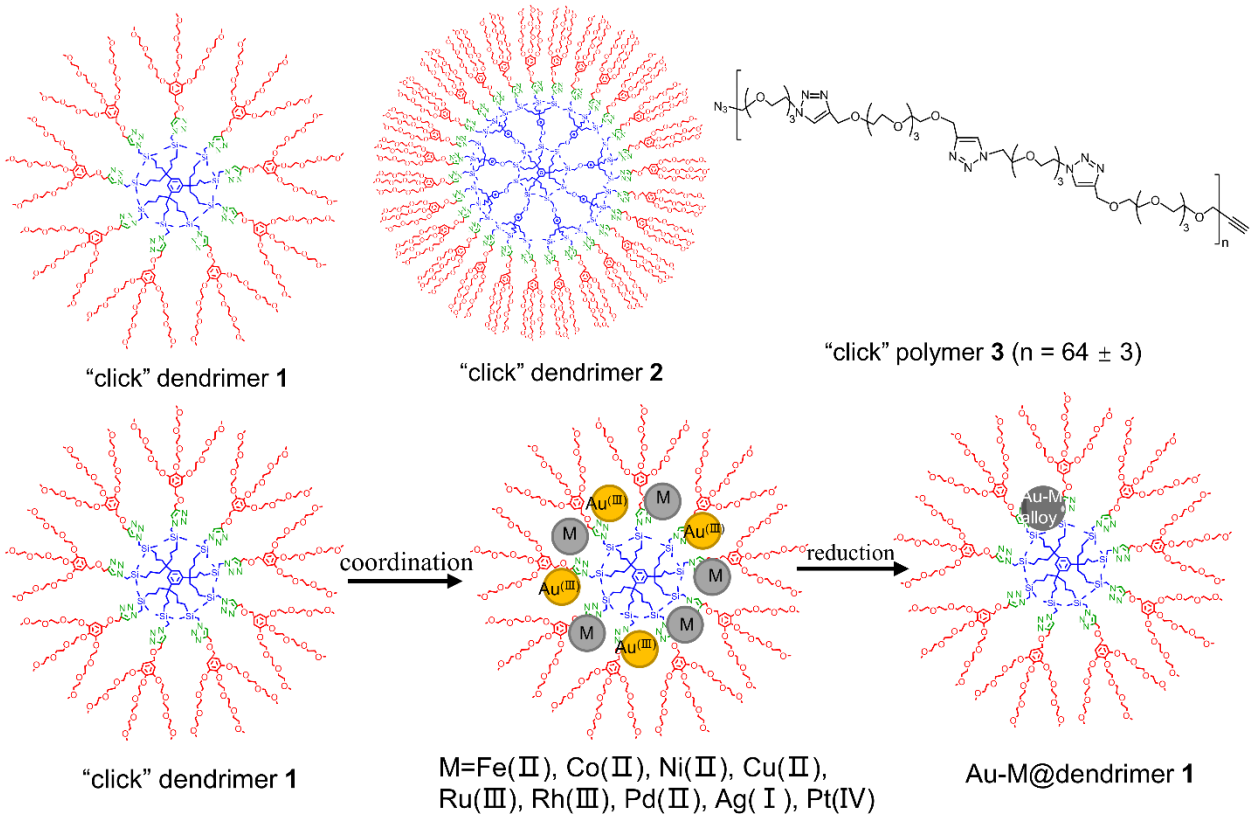

Scheme 1. Syntheses of the macromolecule-stabilized nanocatalysts Au-LTMNP.

Characterization of the nanocatalysts

These alloyed Au-M NPs were characterized by their small sizes measured by Transmission Electron Microscopy (TEM, Figure 1 and S6-S12) and low polydispersity, and the zero-oxidation state of both metals, determined by X-ray Photoelectron Spectroscopy (XPS).

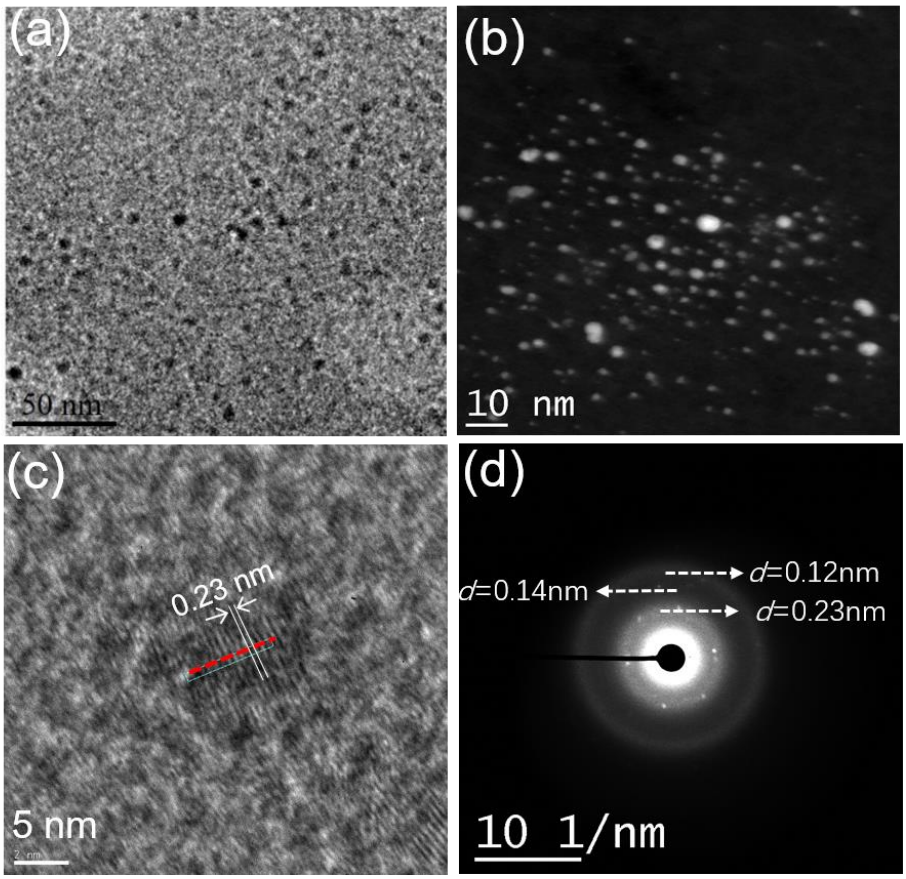

Figure 1. Characterization of Au_1Ru_1@dendrimer **1**, (a) TEM image, (b) HRTEM image, (c) interplanar instance, (d) SEAD image.

For instance, the Au_1Ru_1, Au_1Pt_1 and Au_1Co_1 NPs have a diameter size of 1.48, 1.22 and 2.1 nm respectively, with some polydispersities (Table S1), this small NP size being directed by the selective coordination to the stabilizing tris-triazole tripods with relatively long tethers of the dendrimer **1**. The Au-RhNPs were larger, 3.78 nm in diameter size, and thus stabilized by several dendrimers at their peripheries, which will have consequences on the recycling process (*vide infra*). A good crystallinity of Au_1Ru_1 NPs was confirmed as shown by the clear lattice fringes with 0.23 nm spacing in HRTEM (Figure 1c and 1d), if it is assumed that the crystallographic plane of the Au_1Ru_1 nanoalloy is {111}.[54, 55] Energy dispersive X-ray spectroscopy (EDS) of single Au_1Ru_1 NP showed that the Au and Ru elements were present in the 002 and 003 area (Figure S13). These techniques confirm that and the Au_1Co_1 and Au_1Ni_1NPs also possess alloyed structures (Figure S14-S17). XPS showed that all the nanocatalysts

retained the zero-valence state during catalysis. Since the intradendritic triazole ligands are neutral, surface atoms are indeed expected to be zero-valent (Figure S18-S24).[56]

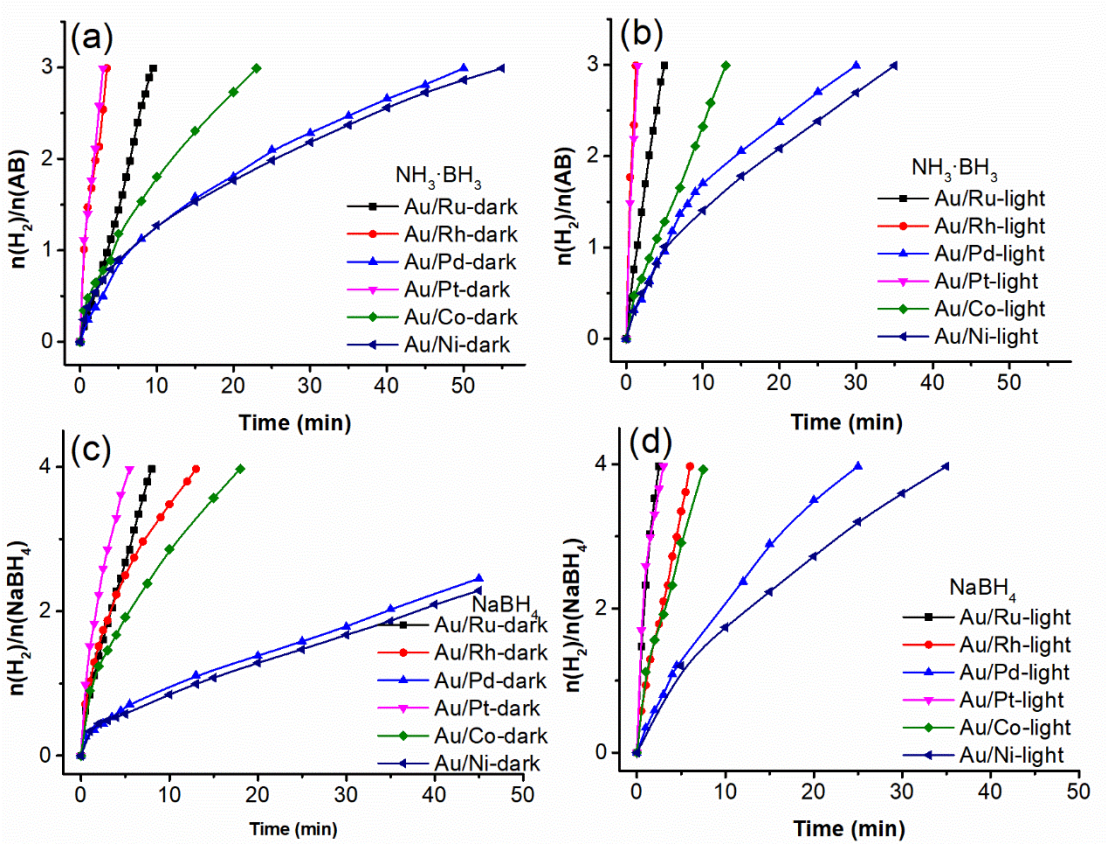

Figure. 2 Plot for molar amount of H_2 generated from AB or $NaBH_4$ hydrolysis vs. time for dendrimer **1**-stabilized Au-LTMNP alloys, (a) AB under dark reaction, (b) AB under visible light, (c) $NaBH_4$ under dark reaction, (d) $NaBH_4$ under visible light. In all the experiments, the reaction conditions are: 1 mmol of AB or $NaBH_4$; 1% mmol MNP; the ratio between Au and M is 1:1; temperature: 25 ± 0.2°C

Hydrolytic dehydrogenation of AB and $NaBH_4$ catalyzed by Au-based bimetallic catalysts.

Under dark conditions, the rates of hydrogen production showed the following order upon AB hydrolysis (Figure 2a): $Au_1Pt_1 > Au_1Rh_1 > Au_1Ru_1 > Au_1Co_1 > Au_1Pd_1 > Au_1Ni_1 > Au$, and for $NaBH_4$ hydrolysis (Figure 2c): $Au_1Pt_1 > Au_1Ru_1 > Au_1Rh_1 > Au_1Co_1 > Au_1Pd_1 > Au_1Ni_1 > Au$. In the dark reactions, alloying with gold had various (positive or, most often, negative) synergistic effects on the catalytic activity vs. the monometallic NP catalysts. Positive synergistic effects were observed essentially

for Au-Co and Au-Pd alloyed nanocatalysts in both AB and $NaBH_4$ hydrolysis reactions in the dark (Table 1). The synergistic effect is due to electronic interaction between the two alloyed metals.[57, 58] The XPS data confirm electronic transfer from Au to Co, and this interaction is beneficial to improve catalytic substrate activation with positive catalytic synergy between these two metals in their nanoalloy. As shown in Figure S23, the binding energy of Au 4f (81.9 eV and 85.5 eV) in the AuCo alloy is shifted to lower value compared to that of AuNPs (83.6 eV and 87.1 eV),[59] while its Co 2p band (779.5 eV and 784.2 eV) is shifted to higher value compared to CoNPs (778.9 eV and 780.6 eV). Conversely, when the shifts of the XPS bands are observed in the same direction towards higher energies for the two metal upon alloying them, electronic transfer is not significant, and there is no catalytic synergy, or a negative synergy due to the dilution of the more active metal in the alloy. This is the case here for AuPt and AuRu. For instance, the Au 4f bands (84.8 and 88.3 eV) of AuPt are shifted to higher values compared to monometallic AuNPs (83.6 eV and 87.1 eV), [59] and the Pt 4f band is also shifted to higher energy from 71.6 and 74.8 eV for PtNPs to 72.6 and 76.0 eV for AuPt (Table S2).

Remarkably, visible-light irradiation boosted the catalysis by all these Au-containing alloys compared to dark reactions, while no light effect was observed with the monometallic NPs (Figure 2b, d, Tables 1 and Figure S25-S29) or bimetallic NPs that did not include Au. Some bimetallic catalysts such as Au-Fe, Au-Cu, and Au-Ag were not effective in quantitatively completing the stoichiometric reactions of equations (1) and (2) (Figure S30). The most spectacular acceleration of Au-LTMNP-catalyzed hydrolysis was observed upon visible-light irradiation of RhNPs and RuNPs that were both alloyed with Au for AB and $NaBH_4$ hydrolysis. As shown in Table S3, for Au_1Ru_1NPs, compared to hydrolytic dehydrogenation of $NaBH_4$ conducted under dark, the TOF value increased from 63.5 to 240.5 mol_{H2} mol_{cat}^{-1} min^{-1} upon visible light irradiation. The TOF value for AB hydrolysis derived by Au-Rh NPs increased from 288.1 to 813.6 mol_{H2} mol_{cat}^{-1} min^{-1} under visible light (Table S3). Increasing the dendrimer generation G_n of the "click" dendrimer stabilizer from G_0 with 27 tethers to G_1 with 81 tethers

has a negative influence on the reaction rates (negative dendrimer generation $_1$pletion of the reaction (Figure

Table 1. Compared TOFs for reactions under dark and visible-light during $NaBH_4$ and AB hydrolysis at 25 ± 0.2°C catalyzed by monometallic and alloyed bimetallic NPs stabilized by the dendrimer **1**.

Catalysts	$NaBH_4$				AB			
	TOF_t[a] (dark)	TOF_t[a] (light)	Synergistic effect [b]	Vis. light effect [c]	TOF^t[a] (dark)	TOF_t[a] (light)	Synergistic effect[b]	Vis. light effect[c]
Au	1.7	1.7	NA[d]	No	1.2	1.2	NA[d]	No
Ru	80	80	NA	No	60	60	NA	No
Au_1/Ru_1	47	178	0.6	3.8	30	67.7	0.5	2.3
Rh	57	57	NA	No	100	100	NA	No
Au_1/Rh_1	33	66	0.6	2	85	240	0.9	2.8
Pd	2.3	2.3	NA	No	1.5	1.5	NA	No
Au_1/Pd_1	6	15	2.6	2.5	6.7	16	4.5	2.4
Pt	133	133	NA	No	133	133	NA	No
Au_1/Pt_1	72	133	0.5	1.85	75	200	0.6	2.7
Co	8	8	NA	No	6	6	NA	No
Au_1/Co_1	22	50	2.75	2.3	17	27	2.8	1.6
Ni	5.2	5.2	NA	No	4	4	NA	No
Au_1/Ni_1	6.1	12.5	1.2	2	5.4	10	1.1	1.9

[a] TOF_t: $mol_{H2\ released}$ / (total $mol_{catalyst}$ × reaction time $_{(min)}$) for all atoms, the unit of TOF_t is $mol_{H2}\ mol_{cat}^{-1}\ min^{-1}$. [b] For reactions in the dark: comparison of the catalytic efficiency between bimetallic NPs and the corresponding monometallic NPs (the better ones). Ratio: TOF_t of the better monometallic NPs/ TOF_t of the alloyed bimetallic NPs. When this ratio is > 1, it shows a positive synergistic effect; conversely, if the ratio is < 1, it shows a negative synergistic effect. [c] Comparison of the efficiencies between the reactions in the dark and with vis. light catalyzed by alloyed bimetallic NPs, expressed as the ratio between TOF_t (alloyed bimetallic NPs under light) and TOF_t (bimetallic NPs under dark). When this effect is >1, it shows a positive vis. light effect. [d] NA: not applicable.

S31, positive dendrimer effect). The Au/Ru and Au/Co and ratios 1/1, 1/2 and 2/1 were tested in the alloys, and the most efficient catalysts were the alloy Au_1Ru_1 and Au_1Co_1 NPs, respectively (Figure S32 and Table S4). Although the low-intensity LED light did not appear to increase the temperature of the reaction system, contribution from the photothermal effect still needed to be considered. The thermometer was located inside the reaction vessel, in order to measure the exact solution temperature. The temperature increase of the aqueous solution containing Au_1Ru_1 catalyst in the presence of visible light irradiation has been measured. A temperature increase of only 1 °C was observed over 10 min of irradiation (Figure S33a), but the efficient catalysts allowed delivery of hydrogen with reactions that were completed after only 1.3 to 4 min depending on the system. There was no significant increase in the hydrogen production rate at 26 °C compared to that at 25 °C (Figure S33b), thus it is concluded that the photothermal effect has no significant contribution to the visible-light induced enhancement of the dehydrogenation reaction.These alloys were also compared with equimolar mixtures of AuNPs and MNPs (M = Ru or Co), and the rate increase upon visible-light irradiation was larger in the alloy than in the mixture of these monometallic NPs (Figure S34 and Table S4). The Au-LTMNPs absorb light in the visible region as shown from their broad plasmon bands observed in the 450-550 nm region in their UV-vis. spectra. Thus, the lack of light-induced acceleration in both AuNP and other monometallic LTMNPs show that the light-induced acceleration of the catalysis is due to the presence of Au in alloys. Upon light absorption by the Au surface atom, a "hot electron" is formed from the Au plasmon and immediately transferred to the substrate-activating Ru or other atom (Au→Ru or Au→M), whatever the electronic delocalization at the NP surface enhancing its catalytic activation efficiency, particularly at corners and edges. Different wavelength irradiations have also been evaluated in the broad range of the plasmon band from 450 to 550 nm. In Figure S35, the catalytic hydrolysis efficiencies of AB and $NaBH_4$ are shown upon 470 nm, 520 nm and 620 nm irradiation. As a result, the 470 nm and 520 nm light irradiations are more efficient to

accelerate the hydrolytic dehydrogenation of AB and $NaBH_4$ catalyzed by Au_1Ru_1@denrimer **1**, respectively.

Recycling of Au_1Ru_1 and Au_1Co_1 catalysts for hydrolysis of AB and $NaBH_4$

Interestingly, after boosting AB or $NaBH_4$ hydrolysis upon visible-light irradiation and complete stoichiometric hydrogen generation, the plasmon band then disappeared, and there was no longer visible-light absorption; then the UV-vis. spectra became flat (Figure 3a and Figure 3d). Upon recycling these catalysts that no longer absorbed visible light, no more light effect was observed upon comparing reactions in the dark and in the presence of light. Surprisingly, however, with most of the alloys the dark reactions upon recycling were faster than the dark reactions of the original alloyed catalysts for both AB and $NaBH_4$ hydrolysis reactions, although not as fast as upon visible-light irradiating the original alloy nanocatalyst (Figure 3b and 3c). Only Au-Pd, Au-Rh and Au-Pt tended to agglomerate after AB hydrolysis, which prevented recycling, contrary to $NaBH_4$ hydrolysis (Table S5). Up to four reaction recycling were carried out with Au_1Ru_1 and Au_1Co_1 with some (but not dramatic) decrease of the rate compared to the initial reaction under visible-light irradiation (Figure 3b). These phenomena were observed for the bimetallic Au_1Ru_1 NPs and Au_1Co_1 NPs tested with both AB hydrolysis and $NaBH_4$ hydrolysis (Figure 3e, 3f and S37). TEM showed that the sizes of the Au-M NPs increased during the light-induced acceleration of the inorganic hydride hydrolysis. For instance, for the Au_1Ru_1 NPs (resp. Au_1Co_1NPs), the NP size increased from 1.5 nm (resp. 2.1 nm) before reaction to 2.5 nm (resp. 5 nm) after visible light reaction (Figure S38-40). During recycling reactions, the NP size no longer increased significantly, however. XPS showed the presence of both Au and Ru at the NP surface before reaction. After reaction in the presence of light, a dramatic decrease in the intensity of Au peaks compared to those of Ru (Figure S41) was observed, in accord with the disappearance of the plasmon band in the UV-vis. spectrum. This reduction in the Au signal hints to an accumulation of the other LTM on the surface of the NP. The disappearance of the plasmon band and the strong decrease of Au at the NP surface both signify removal of Au from the surface and its accumulation on the NP core, reflecting a deep restructuration

from an alloy to a core-shell nanostructure in the course of the light-induced reactions catalyzed by the fresh bimetallic Au-M alloys (Figure 3a). In addition, shifts of the Au 4f and Ru 3d bands are observed upon comparing the XPS spectra before and after reaction (Figure S41). The bands of Au 4f at 84.7 and 88.1 eV before reaction are shifted to lower value (84.0 and 87.6 eV) after reaction, while the Ru 3d bands (284.5 and 286.2 eV) before reaction shifted to higher values (285.1 and 286.7 eV) after reaction. These Au bands are also shifted to lower values compared to those of monometallic AuNP, while the Ru bands are also shifted to higher values compared to those monometallic RuNPs (*vide supra*). This means that electronic transfer from Au to Ru has occurred during the irradiation reaction process, and Ru is also electronic enriched at the expense of Au compared to monometallic Au and Ru NPs. These data all confirm the Au@Ru@dendrimer structure of the restructured bimetallic catalysts following visible-light irradiation. The superior catalytic activity of these restructured Au@Ru NPs compared to the initial Au_1Ru_1 alloy and to the monometallic Ru@dendrimer NPs results from electronic transfer from the Au core to the Ru surface, and the consecutive improved catalytic activity of the core-shell nanocomposite compared to the related alloys has precedents.[60]

The HRTEM/EDS data also show the strong decrease of the Au content at the LTMNP surface (Figure S42a and Table S6). These data indicate that the alloyed NPs progressively transform under the effect of visible light into a core-shell structure leaving almost exclusively only Ru or other non-Au metals at the NP periphery (Figure S42). This transformation that occurred along with a significant increase in size in the presence of the boron hydride and macromolecular triazole was irreversible during further processes for which the structure and size remained essentially constant. It appears that the energy provided by the plasmonic excitation upon visible-light alloy irradiation under these specific reaction conditions allows reaching a more stable thermodynamic state in the core shell Au@M topology than the original nanoalloy state. Since AuNPs are a poor catalyst of these reactions and most other noble LTMNPs are good catalysts,[41] a decrease of the Au content on the alloy surface and an increase of the content of the more active catalyst along the light-induced reactions explain the much better activity upon recycling in the

dark after the restructuration of the catalyst than in the initial alloy (Figure S43-S46). In summary, in the first run of hydrolytic dehydrogenation of AB and sodium borohydride catalyzed by Au-LTMNPs, visible

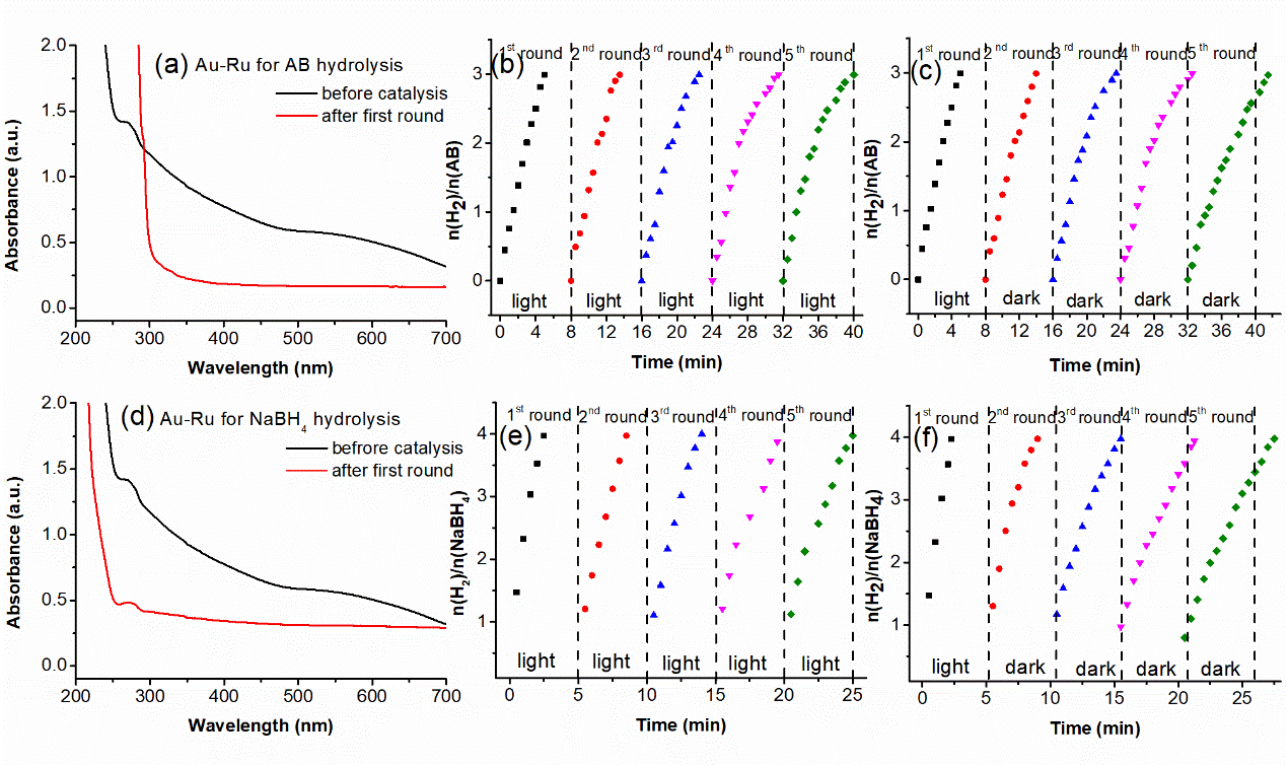

Figure 3 (a) UV-vis. spectra of Au_1Ru_1 for AB hydrolysis before catalysis and after the first catalytic cycle. After further catalysis recycling, the UV-vis. spectra remain the same as after the first cycling. (b) Plot of molar amount of H_2 generated from AB hydrolysis vs. time taken by Au_1Ru_1 during visible light irradiation in the reuse test. (c) Plot of molar amount of H_2 generated from AB hydrolysis vs. time taken by Au_1Ru_1 during the reuse test without visible light in the second cycle. (d) UV-vis. spectra of Au_1Ru_1 for $NaBH_4$ hydrolysis before catalysis and after the first catalytic cycle. After further catalysis recycling, the UV-vis. spectra remained the same as after the first cycle (e) Plot of molar amount of H_2 generated from $NaBH_4$ hydrolysis vs. time taken by Au_1Ru_1 with visible-light irradiation during the reuse test. (f) Plot of molar amount of H_2 generated from $NaBH_4$ hydrolysis vs. time taken by Au_1Ru_1 in the reuse test without visible light in the second cycle. Reaction conditions: amount of AB ($NaBH_4$) used: 1 mmol, temperature: 25 ± 0.2°C

light played two roles: 1) visible-light enhanced catalytic activity upon plasmonic effect of Au surface resulting in the formation and transfer of hot electrons from Au atoms to nearby or other atoms M on the NP surface boosting H_2 release; 2) visible-light induced restructuration of the alloy nanocatalyst to core-shell Au@M topology due to plasmonic hot electron energy provoking formation of the more thermodynamically stable nanomaterial state, in which the Ru or other metal-rich NP surface is much more catalytically active than in the initial Au-containing alloy surface.

Comparison of hydrolysis efficiency of AB and $NaBH_4$ by various nanocatalysts supported by a series of stabilizers

The case of the Au-RhNPs is specific in that, contrary to other Au-LTMNPs these NPs agglomerated after visible-light irradiation, which rendered recycling impossible. This is probably due *inter alia* to the large size of these Au-RhNPs that were stabilized inter-dendritically rather than intra-dendritically, provoking easy agglomeration due to weaker dendritic protection. Except for the Au-RhNPs, dendrimer **1** proved to be an excellent LTMNP support in the catalysis process. Dendrimer **2** could not prevent Au-RhNP agglomeration after catalysis either, due to its small cavities. For all the other Au-LTMNPs, dendrimer **1** was the best support in terms of stabilization, catalysis and recycling, compared to other stabilizers (dendrimer **2**, click polymer **3** and PVP).[53, 61] As shown in table S7, dendrimer **1**, dendrimer **2**, and click polymer **3** made a significant difference between visible-light irradiation and dark reaction. Specifically, the TOF values for hydrolysis of AB and $NaBH_4$ increased at least by a factor of 2 upon shifting reactions from dark to visible light with dendrimer **1**, dendrimer **2** and click polymer **3** as supports, respectively (Table S8). However, there was no change of efficiency between light and dark when PVP was the support, and the catalysts PVP-LTMNP then quickly agglomerated even before the end of reactions. Therefore, the structure of the stabilizer exerts a considerable influence on the photocatalysis. The main structural difference among dendrimer **1**, dendrimer **2**, click polymer **3** and PVP is the presence of the triazole ligands in the first three stabilizers that play a key role in the photocatalysis. The size of

the Au-LTMNP alloy on the triazole-containing stabilizer increased less upon visible-light irradiation, compared to LTMNPs supported on PVP, and consequently Au-LTMNPs stabilized by triazole-containing macromolecular structures can be reused (Figure S47-49, Table 2, S7, S8) contrary to PVP-supported LTMNPs. The dendrimer **1** is the best triazole-containing support, because of the confinement induced by the dendritic tripodal ligands (positive dendritic structure effect) with less steric inhibition than in dendrimer **2**. In summary, the triazole ligand in the stabilizer allows LTMNP stabilization at a small NP size before and during photocatalysis. Therefore, the triazole-containing support facilitates capture of the visible light by coordination to the Au atoms. This tripodal coordination increases electronic density on the NP, thereby accelerating plasmonic generation of hot electrons,[53, 56] and the optimized stereo-electronic functions of the triazole-containing stabilizer are best insured by the NP-encapsulating dendrimer **1**.

Table 2. Comparison of the different stabilizers for dark and visible-light irradiation derived by Au_1Ru_1 catalyst upon $NaBH_4$ hydrolysis reactions at 25 ± 0.2°C

Supports	TOF_t[a] ($NaBH_4$ under dark)	TOF_t [a] ($NaBH_4$ under light)	TOF_t [a] (AB under dark)	TOF_t[a] (AB under dark)	recycling
Dendrimer **1**	63.5	240.5	40.5	101.4	YES
Dendrimer **2**	51.6	96.7	34.0	68.1	YES
"Click" polymer **3**	27.5	55.3	16.8	31.1	YES
PVP	123.4	123.4	84.0	84.0	NO

[a] $TOF_t = mol_{H2\ released} / (surface\ mol_{catalyst} \times reaction\ time_{(min)})$

Proposed mechanism

The light-induced reaction mechanism must take into account both effects of light on these nanocatalyzed hydrogen evolution reactions: (i) light-induced acceleration of hydrogen release, and (ii) light-induced nanoalloy restructurarion to core@shell NP. Both light effects are causing reaction acceleration at the very beginning of the reaction, whereas by the end on the reaction only the restructuration alloy → Au core@Ru is the cause of hydrogen release acceleration compared to catalysis by the nanoalloy in the dark. Thus, the plasmon-induced acceleration progressively decreases along the reaction with the progressively growing effect of decrease of Au proportion and increase of Ru proportion

on the NP surface. In order to distinguish between these two effects of light, the effect of the time of light irradiation on the time necessary to obtain complete hydrogen evolution was investigated. For instance with $NaBH_4$ (Figure S50a), complete hydrogen evolution was obtained after 2.5 min of light irradiation, whereas 9 min was necessary in the dark. It was found that one or two min of visible-light irradiation was not sufficient, but only with 2.5 min of visible-light irradiation was complete evolution obtained in 3 min. Consequently, during the last 0.5 min necessary to obtain complete hydrogen evolution from AB, the light had no more effect on the reaction, and the regime was the same as during the recycling, i.e. reaction acceleration compared to reaction of the alloy-nanocatalyzed reaction is exclusively due to Ru being in higher proportion than Au on surface of the core Au@Ru shell NP than on the surface of the initial alloy.

Concerning the reaction mechanism of AB hydrolytic hydrogen release in the dark, let us recall that one of the hydrogen atoms from H_2 comes from AB and the other one from water. [62-64] The kinetic isotope effect (KIE: k_H/k_D) is an effective way to identify the rate-determining step (RDS) of a reaction.[65, 66] The proposed mechanism earlier with AB for dark reactions was suggested to involve cleavage of a water O-H bond in the rate-limiting step (RLS) based on high values of the KIE values between 2.46 [50] and 2.49 [30] using D_2O combined with low values of KIE using NH_3BD_3 such as 1.33.[30] With Au_1Ru_1@dendrimer **1** in the dark, the KIE found with D_2O was 2.25 (Figure S51), which is consistent with earlier studies confirming a primary KIE leading to an analogous suggestion of water O-H bond cleavage in the RLS. In the presence of light, this KIE value raised to 3.00, which even more clearly reflects water bond breaking in the RLS. Interestingly, in the recycling experiment, the KIE value found raised to 3.38 pointing an additional KIE increase compared to the initial experiment under visible light (Figure S51), which is due both to the increased activity of the Ru atoms on the alloy surface and to the light-induced NP restructuration bringing a higher proportion of Ru atoms on the NP surface. In the presence of light, this electron density on Ru atoms is strongly enriched by the additional hot electron transmitted from the Au plasmon. Visible light accelerates the reaction, and the KIE with D_2O should be enhanced compared

to the KIE of the dark reaction; this was indeed found. Overall, the cleavage of the water O-H bond in the species NP-H...H-OH in the RLS in the presence of visible light for AB hydrolysis appears more clearly, partly due to the privileged role of Ru atoms in this oxidative addition compared to those of other elements such as Au and Ni. Oxidative addition of the water O-H bond can be achieved by a single Ru atom or by two adjacent Ru atoms of the NP surface.[67, 68] This RLS follows the fast B-H bond activation of AB on the NP surface that appears independent from the RLS step due to the insignificant hydrogen bonding between neutral AB and water (Scheme 2, top).

After reductive elimination of both H_2 and $[NH_3BH_2OH]$, the same step would occur again with the later, finally leading to the formation from AB of 3 mol H_2 and $[NH_3B(OH)_3]$, then $[NH_3B(OH)_3]$ further hydrolyzed to stable $[NH_4B(OH)_4]$ (Scheme 2).

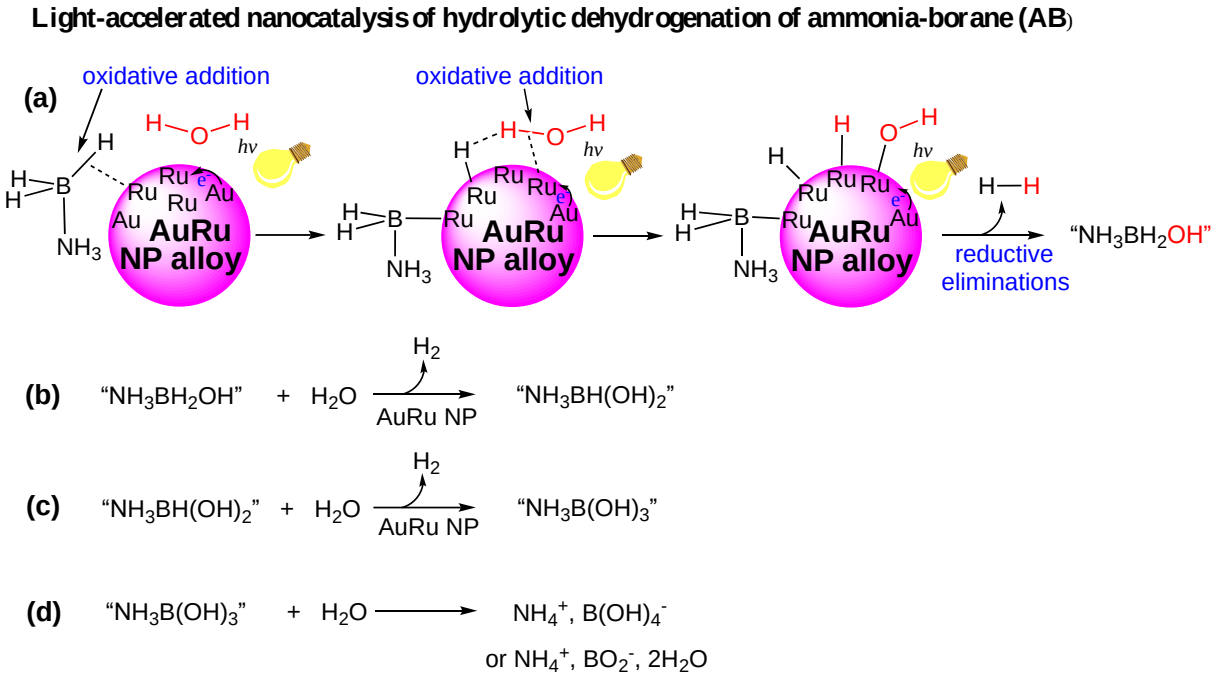

Scheme 2. Suggested mechanism for the visible-light-accelerated hydrolytic dehydrogenation of AB nanocatalyzed by Au_1Ru_1@dendrimer **1**.

This mechanism seems relatively similar for $NaBH_4$ and AB. Indeed, with $NaBH_4$ the KIE obtained using D_2O was 2.25 in the dark, 3.40 under visible light and 3.8 in the recycling (Figure S52a), which follows the same trends as with AB. Experiments with $NaBD_4$ led to KIE of 1 in the dark, and 1.13 in

recycling (Figure. S52b), indicating that $NaBH_4$ is not involved in the RLS and that no restructuration occurs along the experiment in the absence of light.

On the other hand, experiments in the presence of visible light led to a KIE of 2.2, whereas 2.6 was obtained in the recycling (Figure S52b). This shows that, in the presence of visible-light irradiation, both visible-light and light-induced alloy → Au core @Ru shell restructuration boost the activity of the Ru atoms that synergistically activate both the B-H and O-H bonds in the RLS in a concerted way, although the O-H bond is stronger (493 kJ mol^{-1}) [61] than the B-H bond (430 kJ mol^{-1}).[69] This synergy can be taken into account by the strong H-bonding between a hydridic hydrogen and H_2O that brings the $NaBH_4$...H_2O ensemble onto the NP surface together with the fact that the Ru atoms, that are strong X-H bond activators, activate both bonds in the same step, also because of O-H bond weakening by hydrogen bonding, contrary to weaker bond activators among the transition metals that are more selective (Scheme 3).[65, 66, 68]

Light-accelerated nanocatalysis of hydrolytic dehydrogenation of sodium borohydride

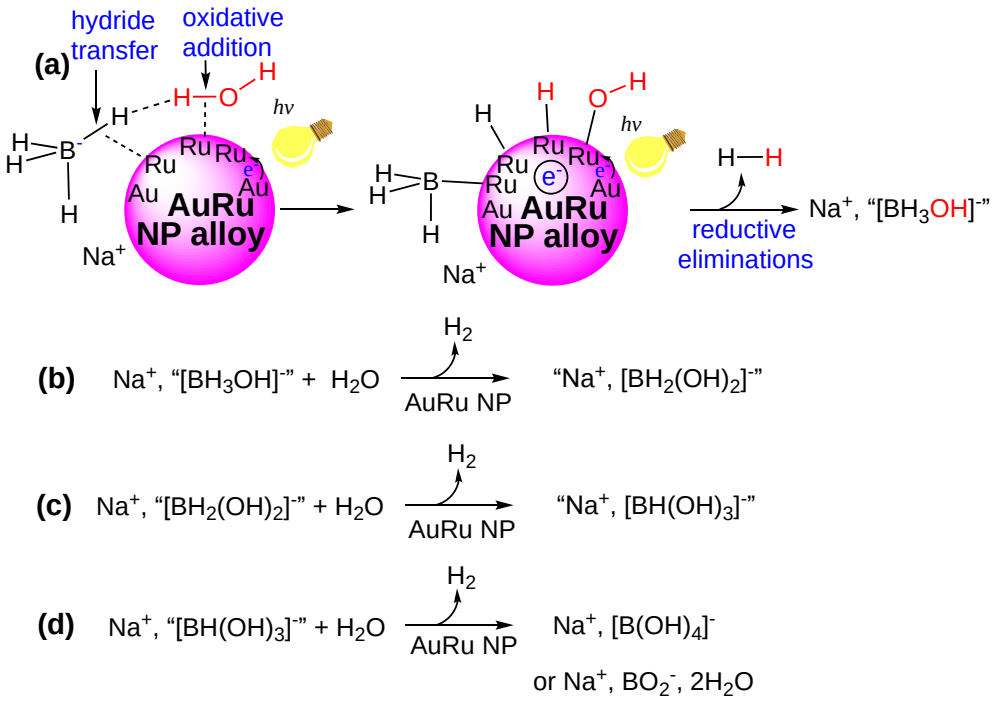

Scheme 3. Suggested mechanism for the visible-light-accelerated hydrolytic dehydrogenation of $NaBH_4$ nanocatalyzed by Au_1Ru_1@dendrimer **1**.

$NaBH_4$ is hydrolyzed, to 4 mol H_2, much more easily than AB when Au_1Ru_1 and Au_1Co_1 are the nanocatalysts (Figure S52). This is verified in terms of performances. The TOF values of AB hydrolysis catalyzed by Au_1Ru_1 and Au_1Co_1were previously found to be 101.4 and 60.0 $mol_{H2}\cdot molcatal.^{-1}\cdot min^{-1}$, respectively, which is inferior, under the same conditions, to those found with $NaBH_4$ for Au_1Ru_1 and Au_1Co_1 of 240.5 and 111.1 $mol_{H2}\cdot molcatal.^{-1}\cdot min^{-1}$, respectively.

CONCLUSION

It has been shown here that visible light boosts the Au-based alloyed nanocatalysts Au-LTMNPs (LTM = Ru, Co, Rh, Ni, and Pt) with a series of triazole-containing macromolecular stabilizers as supports for H_2 production from dehydrogenation reaction of aqueous solutions of the hydrogen-rich boron derivatives AB and $NaBH_4$. Dendrimer **1**-stabilized Au_1Ru_1, $Au_1Pt_1$and Au_1Rh_1NPs showed remarkably high visible-light effects and efficiencies for these hydrolysis reactions, and Au_1Ru_1 was recycled four times in dark reactions. Thus, Ru combines the advantages of being by far the cheapest noble metal and showing excellent light-acceleration effects, efficiencies and recyclabilities in both AB and $NaBH_4$ hydrolysis reactions. In fact, there are two light effects that both favor H_2 evolution from these hydrogen-rich boron derivatives. The first one is photocatalytic, i. e. the light absorption by the Au plasmon produces hot electrons that are transferred to one or several adjacent Ru atoms boosting substrate activation efficiency to produce H_2. The second visible-light effect simultaneously causes progressive alloy → Au core@Ru (or other metal) shell restructuration resulting in higher activity of the surface Ru atoms (or other atoms) than at the alloy surface of the original NP. For instance, with the Au_1Ru_1 alloy, this restructuration is accomplished in 2.5 min, whereas the total time needed for H_2 evolution is 2.5 min. Consistently, the recycling experiment in the dark, following the initial light-accelerated reaction, takes some more time than the latter, but less time than with the original nanocatalyst in the dark. This is explained by the

visible-light-induced restructuration from alloy to Au@Ru or Au@M core-shell NPs. Au-Co, although less active than the alloyed Au-noble-metal photocatalysts, showed excellent light effect and was the best alloyed Au-earth-abundant metal photocatalyst for both reactions and, as Au-Ni, was recyclable. The presence of the triazole ligand in the macromolecular structure is a key factor in light enhancement of H_2 evolution and catalyst recycling, the optimized structure being the dendrimer **1**, more efficient than dendrimer **2** and polymer **3** because of its ideal stereo-electronic effects on the NP stabilization and photocatalytic activity of the Au-LTMNPs. Finally, the enhanced KIE values obtained using D_2O under visible-light irradiation and recycling in the dark compared to those obtained in dark reactions of the alloys confirm the strong implication of the water oxidative addition in the RLS for both AB and $NaBH_4$ hydrolytic reactions. Nevertheless, with $NaBH_4$ (only), high KIE values obtained using $NaBD_4$ show that the initial hydride transfer for this substrate to the NP surface also intervenes in a concerted way with the water O-H cleavage in the RLS due to initial strong hydrogen bonding with water. These photocatalysts show superior activity compared to previously reported AB hydrolysis plasmonic metal-based photocatalysts with or without semiconductor (Table S9). It is believed that these concepts and findings will find extension to new improved H_2 generation systems and other redox-photocatalyzed transformations of small molecules.

ASSOCIATED CONTENT

Supporting Information.

Materials and methods, nanomaterial characterization, kinetics of hydrolysis of boron hydrides, and supplementary references (25 pages).

AUTHOR INFORMATION

Corresponding Author

didier.astruc@u-bordeaux.fr

Notes

The authors declare no conflict of interest.

ACKNOWLEDGMENT

Helpful remarks of the reviewers and financial support from the China Scholarship Council (CSC) (PhD grant to N. K.), the National Science Centre of Poland under the program OPUS (E.C. 2019/35/B/ST5/00248 and S.M: 2019/33/B/ST5/01495), the Centre National de la Recherche Scientifique (CNRS), and the University of Bordeaux (D.A. and J.-L.P.) are gratefully acknowledged.

REFERENCES

Present addresses: Dr Rodrigue Djeda: Laboratoire de Chimie Organique et de Substances Naturelles, Université Félix Houphouët Boigny, 22 BP 582 Abidjan 22, Ivory Coast. Dr Fangyu Fu: Key Laboratory of Cluster Science of Ministry of Education, School of Chemistry and Chemical Engineering, Beijing Institute of Technology, 100081 Beijing, People's Republic of China.

(1) Oshchepkov, A. G.; Braesch, G.; Bonnefont, A.; Savinova, E. R.; Chatenet, M. Recent Advances in the Understanding of Nickel-Based Catalysts for the Oxidation of Hydrogen-Containing Fuels in Alkaline Media. *ACS Catal.* **2020**, *10*, 7043-7068.

(2) Luo, N.; Hou, T.; Liu, S.; Zeng, B.; Lu, J.; Zhang, J.; Li, H.; Wang, F. Photocatalytic Coproduction of Deoxybenzoin and H-2 through Tandem Redox Reactions. *ACS Catal.* **2020**, *10*, 762-769.

(3) Fujishima, A.; Honda, K.; Electrochemical Photolysis of Water at a Semiconductor Electrode. *Nature* **1972,** *238,* 37-38.

(4) Deng, Y.; Tang, L.; Feng, C.; Zeng, G.; Chen, Z., Wang, J.; Feng, H.; Peng, B.; Liu, Y.; Zhou, Y. Insight into the Dual-Channel Charge-Charrier Transfer Path for Nonmetal Plasmonic Tungsten Oxide

Based Composites with Boosted Photocatalytic Activity under Full-Spectrum Light. *Appl. Catal. B* **2018**, *235*, 225-237.

(5) Shiraishi, Y.; Takii, T.; Hagi, T.; Mori, S.; Kofuji, Y.; Kitagawa, Y.; Tanaka, S.; Ichikawa, S.; Hirai, T. Resorcinol-Formaldehyde Resins as Metal-Free Semiconductor Photocatalysts for Solar-to-Hydrogen Peroxide Energy Conversion. *Nat. Mater*. **2019**, *18*, 985-993.

(6) Rej, S.; Mascaretti, L.; Santiago, E. Y.; Tomanec, O.; Kment, S.; Wang, Z.; Zboril, R.; Fornasiero, P.; Govorov, A. O.; Naldoni, A. Determining Plasmonic Hot Electrons and Photothermal Effects during H-2 Evolution with TiN-Pt Nanohybrids. *ACS Catal.* **2020**, *10*, 5261-5271.

(7) Balayeva, N. O.; Mamiyev, Z.; Dillert, R.; Zheng, N.; Bahnemann, D. W. Rh/TiO_2-Photocatalyzed Acceptorless Dehydrogenation of N-Heterocycles upon Visible-Light Illumination. *ACS Catal.* **2020**, *10*, 5542-5553.

(8) Wang, Y.; Shen, G.; Zhang, Y.; Pan, L.; Zhang, X.; Zou, J.J. Visible-Light-Induced Unbalanced Charge on NiCoP/TiO_2 Sensitized System for Rapid H_2 Generation from Hydrolysis of Ammonia Borane. *Appl. Catal. B* **2020**, *260*, 118183.

(9) Wang, C.; Astruc, D. Nanogold Plasmonic Photocatalysis for Organic Synthesis and Clean Energy Conversion. *Chem. Soc. Rev*. **2014**, *43,* 7188-7216.

(10) Zheng, Z.; Tachikawa, T.; Majima, T.; Plasmon-Enhanced Formic Acid Dehydrogenation Using Anisotropic Pd-Au Nanorods Studied at the Single-Particle Level. *J. Am. Chem. Soc.* 2015, *137*, 948-957.

(11) Linic, S.; Aslam, U.; Boerigter, C.; Morabito, M. Photochemical Transformations on Plasmonic Metal Nanoparticles. *Nat. Mater.* **2015**, *14,* 567-576.

(12) Zada, A.; Muhammad, P.; Ahmad, W.; Hussain, Z.; Ali, S.; Khan, M.; Khan, Q.; Maqbool, M. Surface Plasmonic-Assisted Photocatalysis and Optoelectronic Devices with Noble Metal Nanocrystals: Design, Synthesis, and Applications. *Adv. Funct. Mater*. **2019**, *30,* 1906744

(13) Wen, M.; Kuwahara, Y.; Mori, K.; Yamashita, H.; Enhancement of Catalytic Activity over AuPd Nanoparticles Loaded Metal Organic Framework under Visible Light Irradiation. *Top. Catal.* **2016**, *59,* 1765-1771.

(14) Rej, S.; Hsia, C.; Chen, T.; Lin, F.; Huang, J.; Huang, M. H.; Hydrogen Evolution Facet-Dependent and Light-Assisted Efficient Hydrogen Evolution from Ammonia Borane Using Gold–Palladium Core–Shell Nanocatalysts. *Angew. Chem., Int. Ed.* **2016**, *55*, 7222-7226.

(15) Verma, P.; Yuan, K.; Kuwahara, Y.; Mori, K.; Yamashita, H. Enhancement of Plasmonic Activity by Pt/Ag Bimetallic Nanocatalyst Supported on Mesoporous Silica in the Hydrogen Production from Hydrogen Storage Material. *Appl. Catal. B* **2018**, *223*, 10-15.

(16) Gelle, A.; Jin, T.; Garza, de la L.; Price, G. D.; Besteiro, L. V.; Moores, A.; Applications of Plasmon-Enhanced Nanocatalysis to Organic Transformations. *Chem. Rev*. **2020**, *120,* 986-1041.

(17) Sun, D.; Hao, Y.; Wang, C.; Zhang, X.; Yu, X.; Yang, X.; Li, L.; Lu, Z.; Shang, W. TiO_2-CdS Supported CuNi Nanoparticles as a Highly Efficient Catalyst for Hydrolysis of Ammonia Borane under Visible-Light Irradiation. *Int. J. Hydrog. Energy* **2020**, *45*, 4390-4402.

(18) Wu, Y.; Sun, Y.; Fu, W.; Meng, X.; Zhu, M.; Ramakrishna, S.; Dai, Y. Graphene-Based Modulation on the Growth of Urchin-like $Na_2Ti_3O_7$ Microspheres for Photothermally Enhanced H_2 Generation from Ammonia Borane. *ACS Appl. Nano Mater.* **2020**, *3*, 2713-2722.

(19) Jo, S.; Verma, P.; Kuwahara, Y.; Mori, K.; Choi, W.; Yamashita, H.; Enhanced Hydrogen Production from Ammonia Borane Using Controlled Plasmonic Performance of Au Nanoparticles Deposited on TiO_2. *J. Mater. Chem. A* **2017**, *5*, 21883-21892.

(20) Kurnaravel, V.; Mathew, S.; Bartlett, J.; Pillai, S. C. Photocatalytic Hydrogen Production Using Metal Doped TiO_2: A Review of Recent Advances. *Appl. Catal. B* **2019**, *244*, 1021-1064.

(21) Gao, M.; Yu, Y.; Yang, W.; Li, J.; Xu, S.; Feng, M.; Li, H. Ni Nanoparticles Supported on Graphitic Carbon Nitride as Visible Light Catalysts for Hydrolytic Dehydrogenation of Ammonia Borane. *Nanoscale* **2019**, *11*, 3506-3513.

(22) Zhang, H.; Gu, X.; Song, J. Co, Ni-Based Nanoparticles Supported on Graphitic Carbon Nitride Nanosheets as Catalysts for Hydrogen Generation from the Hydrolysis of Ammonia Borane under Broad-Spectrum Light Irradiation. *Int. J. Hydrog. Energy* **2020**, *45*, 21273-21286.

(23) Zhang, H.; Gu, X.; Liu, P.; Song, J.; Cheng, J.; Su, H. Highly Efficient Visible-Light-Driven Catalytic Hydrogen Evolution from Ammonia Borane Using Non-Precious Metal Nanoparticles Supported by Graphitic Carbon Nitride. *J. Mater. Chem. A* **2017**, *5*, 2288-2296.

(24) Zhu, Q.-L.; Xu, Q. Liquid Organic and Inorganic Chemical Hydrides for High-Capacity Hydrogen Storage. *Energy Environ. Sci.* **2015**, *8*, 478-512.

(25) Akbayrak, S.; Ozkar, S. Ammonia Borane as Hydrogen Storage Materials. *Int. J. Hydrog. Energy* **2018**, *43*, 18592-18606.

(26) Wang, C.; Wang, Q.; Fu, F., Astruc, D. Hydrogen Generation upon Nanocatalyzed Hydrolysis of Rich Boron Derivatives: Recent Developments. *Acc. Chem. Res.* **2020**, *53*, 000, doi.org/10.1021/acs.accounts.0c00525

(27) Kumar, R.; Karkamkar, A.; Bowden, M.; Autrey, T. Solid-State Hydrogen Rich Boron-Nitrogen Compounds for Energy Storage, *Chem. Soc. Rev.* **2019**, *48,* 5350-5380.

(28) Asefa, T.; Koh, K.; Yoon, C. W. CO_2- Mediated H_2 Storage-Release with Nanostructured Catalysts: Recent Progresses, Challenges, and Perspectives. *Adv. Energy Mater.* **2019**, *9,* 1901158.

(29) Alpaydin, C. Y.; Gülbay, S. K.; Colpan, G. O. A Review on the Catalysts Used for Hydrogen Production from Ammonia Borane. *Int. J. Hydrog. Energy* **2020**, *45,* 3414-3434.

(30) Wang, C.; Tuminetti, J.; Wang, Z.; Zhang, C.; Ciganda, R.; Moya, S.; Ruiz, J.; Astruc, D. Hydrolysis of Ammonia-Borane over Ni/ZIF-8 Nanocatalyst: High Efficiency, Mechanism, and Controlled Hydrogen Release. *J. Am. Chem. Soc*. **2017**, *139,* 11610-11615.

(31) Rossin, A.; Tuci, G.; Luconi, L.; Giambastiani, G. Metal-Organic Frameworks as Heterogeneous Catalysts in Hydrogen Production from Lightweight Inorganic Hydrides. *ACS Catal.* **2017**, *7*, 5035-5045.

(32) Fu, F.; Wang, C.; Wang, Q.; Martinez-Villacorta, A. M.; Escobar, A.; Chong, H.; Wang, X.; Moya, S.; Salmon, L.; Fouquet, E.; Ruiz, J.; Astruc, D. Highly Selective and Sharp Volcano-Type

Synergistic Ni_2Pt@ZIF-8-Catalyzed Hydrogen Evolution from Ammonia Borane Hydrolysis. *J. Am. Chem. Soc.* **2018**, *140,* 10034-10042.

(33) Lu, N.; Zhang, Z.; Wang, Y.; Liu, B.; Guo, L.; Wang, L.; Huang, J.; Liu, K.; Dong, B. Direct Evidence of IR-Driven hot Electron Transfer in Metal-Free Plasmonic $W_{18}O_{49}$/Carbon Heterostructures for Enhanced Catalytic H_2 Production. *Appl. Catal. B* **2018**, *233,* 19-25.

(34) Zhang, J.; Chen, W.; Ge, H.; Chen, C.; Yan, W.; Gao, Z.; Gan, J.; Zhang, B.; Duan, X.; Qin, Y.; Synergistic Effects in Atomic-Layer-Deposited $PtCo_x$/CNTs Catalysts Enhancing Hydrolytic Dehydrogenation of Ammonia Borane. *Appl. Catal. B* **2018**, *235*, 256-263.

(35) Yao, K.; Zhao, C.; Wang, N.; Li, T.; Lu, W.; Wang, J. An Aqueous Synthesis of Porous PtPd Nanoparticles with Reversed Bimetallic Structures for Highly Efficient Hydrogen Generation from Ammonia Borane Hydrolysis. *Nanoscale* **2020**, *12*, 638-647.

(36) Wang, Y.; Shen, G.; Zhang, Y.; Pan, L.; Zhang, X.; Zou, J.-J Visible-Light-Induced Unbalanced Charge on NiCoP/TiO_2 Sensitized System for Rapid H_2 Generation from Hydrolysis of Ammonia Borane. *Appl. Catal. B* **2020**, *260*, 118183.

(37) de Vries, J. G.; Elsevier, C. J.; *In the Handbook of Homogeneous Hydrogenation*; Wiley-VCH: Weinheim, Germany 2007.

(38) Bronstein L. M.; Shiffrina, Z.; Dendrimers as Encapsulating, Stabilizing, and Directing Agents for Inorganic Nanoparticles, *Chem. Rev*. **2011**, *111*, 5301-5344.

(39) Myers, V. S.; Weir, M. G.; Carino, E. V.; Crooks, R. M. Dendrimer-Encapsulated Nanoparticles: New Synthetic and Characterization Methods and Catalytic Applications, *Chem. Sci.* **2011**, *2,* 1632-1646.

(40) Imaoka, T.; Kitazawa, H.; Chun, T. W.-J.; Yamamoto, K.; Finding the Most Catalytically Active Platinum Clusters with Low Atomicity, *Angew. Chem., Int. Ed.* **2015**, *54*, 9810-9815.

(41) Li, Z.; He, T.; Matsumura, D.; Miao, S.; Wu, A.; Liu, L.; Wu, G.; Chen, P. Atomically Dispersed Pt on the Surface of Ni Particles: Synthesis and Catalytic Function in Hydrogen Generation from Aqueous Ammonia-Borane. *ACS Catal.* **2017**, *7*, 6762-6769.

(42) Samantaray, M. K.; Pump, E.; Bendjeriou-Sedjerari, A.; D'Elia, V.; Pelletier, J. D. A.; Guidotti, M.; Psaro, R.; Basset, J. M. J. Surface Organometallic Chemistry in Heterogeneous Catalysis. *Chem. Soc. Rev.* **2018**, *47*, 8403-8437.

(43) Liu, L.; Corma, A.; Metal Catalysts for Heterogeneous Catalysis: From Single Atoms to Nanoclusters and Nanoparticle. *Chem. Rev*. **2018**, *118*, 4981-5079.

(44) Astruc, D. Introduction: Nanoparticles in Catalysis. *Chem. Rev*. **2020**, *120,* 461-463.

(45) Sankar, M.; He, Q.; Engel, R. V.; Sai, M. A.; Logsdail, A. J.; Roldan, A.; Willock, D. J.; Agarwal, N.; Kiely, C.; Hutchings, G. Role of the Support in Gold-Containing Nanoparticles as Heterogeneous Catalysts. *J. Chem. Rev.* **2020**, *120,* 3890-3938.

(46) Xie, C.; Niu, Z.; Kim, D.; Li, M.; Yang, P. Surface and Interface Control in Nanoparticle Catalysis. *Chem. Rev*. **2020**, *120,* 1184-1249.

(47) Li, Y.; Cain, J. D.; Hanson, E. D.; Murthy, A. A.; Hao, S.; Shi F.; Li, Q.; Wolverton, C.; Chen, Q.; Dravid, V. P.; Au@MoS_2 Core–Shell Heterostructures with Strong Light–Matter Interactions. *Nano Lett.* **2016**, *16*, 7696-7702.

(48) Mori, K.; Verma, P.; Hayashi, R.; Fuku, K.; Yamashita, H. Color-Controlled Ag Nanoparticles and Nanorods within Confined Mesopores: Microwave-Assisted Rapid Synthesis and Application in Plasmonic Catalysis under Visible-Light Irradiation. *Chem. Eur. J.* **2015**, *21,* 11885-11893.

(49) Wang, Q.; Fu, F.; Yang, S.; Moro, M. Martinez; Ramirez, M. de los A.; Moya, S.; Salmon, L.; Ruiz, J.; Astruc, D. Dramatic Synergy in CoPt Nanocatalysts Stabilized by "Click" Dendrimers for Evolution of Hydrogen from Hydrolysis of Ammonia Borane. *ACS Catal.* **2019**, *9,* 1110-1119.

(50) Daniel, M. C.; Astruc, D.; Gold Nanoparticles: Assembly, Supramolecular Chemistry, Quantum-Size-Related Properties, and Applications toward Biology, Catalysis, and Nanotechnology. *Chem. Rev.* **2004**, *104,* 293-346.

(51) Jiang, N.; Zhuo, X.; Wang, J.; Active Plasmonics: Principles, Structures, and Applications. *Chem. Rev.* **2018**, *118,* 3054-3099.

(52) Boisselier, E.; Diallo, K. A.; Salmon, L.; Ornelas, C.; Ruiz, J.; Astruc, D. Encapsulation and Stabilization of Gold Nanoparticles with "Click" Polyethyleneglycol Dendrimers. *J. Am. Chem. Soc.* **2010**, *132,* 2729-2742.

(53) Deraedt, C.; Rapakousiou, A.; Wang, Y.; Salmon, L.; Bousquet, M.; Astruc, D.; Multi-Function Redox Polymers: Electrochrome, Polyelectrolyte, Sensor, Electrode Modifier, Nanoparticle Stabilizer and Catalyst Template. *Angew. Chem., Int. Ed.* **2014**, *53,* 8445-8449

(54) Goriachko, A.; Over, H. Subtle Nanostructuring of the Au/Ru(0001) Surface. *Nanoscale Res. Lett.* **2018**, *13*, 203.

(55) Zhang, Q.; Kusada, K.; Wu, D.; Yamamoto, T.; Toriyama, T.; Matsumura, S.; Kawaguchi, S.; Kubota, Y.; Kitagawa, H.; Selective Control of fcc and hcp Crystal Structures in Au-Ru Solid-Solution Alloy Nanoparticles. Nat. Commun. **2018**, 9,118612.

(56) Wang, D.; Astruc, D. Dendritic Catalysis-Basic Concepts and Recent Trends. *Coord. Chem. Rev.* 257 **2013**, *257*, 2317-2334.

(57) Zhang, S.; Li, M.; Zhao, J.; Wang, H.; Zhu, X.; Han, J.; Liu, X. Plasmonic AuPd-Based Mott-Schottky Photocatalyst for Synergistically Enhanced Hydrogen Evolution from Formic Acid and Aldehyde. *Appl. Catal. B* **2019**, *252*, 24-32.

(58) Zhang, S.; Wang, H.; Tang, L.; Li, M.; Tian, J.; Cui, Y.; Han, J.; Zhu, X.; Liu, X. Sub 1 nm Aggregation-Free AuPd Nanocatalysts Confined inside Amino-Functionalized Organosilica Nanotubes for Visible-Light-Driven Hydrogen Evolution from Formaldehyde. *Appl. Catal. B* **2018**, *220*, 303-313.

(59) Liu, X.; Ruiz, J.; Astruc, D. Compared Catalytic Efficiency of Click-Dendrimer-Stabilized Late Transition Metal Nanoparticles in 4-Nitrophenol Reduction. *J. Inorg. Organomet. Polym. Mater*. **2018**, *28*, 399-406.

(60) Tedsree, K.; Li, T.; Jones, S.; Chan, C. W. A.; Yu, K. M. K.; Bagot, P. A. J.; Marquis, E. A.; Smith, G. D. W.; Tsang, S. C. E. Hydrogen Production from Formic Acid Decomposition at Room Temperature Using A Ag-Pd Core-Shell Nanocatalyst. *Nat. Nanotechnol*. **2011**, *6,* 302-307.

(61) Liu, X.; Gregurec, D.; Irigoyen, J.; Martinez, A.; Moya, S.; Ciganda, R.; Hermange, P.; Ruiz, J.; Astruc, D.; Precise Localization of Metal Nanoparticles in Dendrimer Nanosnakes or Inner Periphery and Consequences in Catalysis. *Nat. Commun.* **2016**, *7*, 1-8.

(62) Rablen, P. R. Large Effect on Borane Bond Dissociation Energies Resulting from Coordination by Lewis Bases. *J. Am. Chem. Soc.* **1997**, *119*, 8350-8360.

(63) Westheimer, F. H. The Magnitude of the Primary Kinetic Isotope Effect for Compounds of Hydrogen and Deuterium. *Chem. Rev.* **1961**, *61, 3,* 265-273.

(64) Zhan, W. W.; Zhu, Q. L.; Xu, Q. Dehydrogenation of Ammonia Borane by Metal Nanoparticle Catalysts. A*CS Catal.* **2016**, *6*, 6892-6905.

(65) Li, Z.; He, T.; Liu, L.; Chen, W.; Zhang, M.; Wu, G.; Chen, P. Covalent Triazine Framework Supported Non-Noble Metal Nanoparticles with Superior Activity for Catalytic Hydrolysis of Ammonia Borane: from Mechanistic Study to Catalyst Design. *Chem. Sci*. **2017**, *8*, 781-788.

(66) Astruc, D. *Organometallic Chemistry and Catalysis*. Springer, Berlin, **2007**, Chap. 3.

(67) Axet, M. R.; Philippot, K. Catalysis with Colloidal Ruthenium Nanoparticles. *Chem. Rev.* **2020**, *120*, 1085-1145.

(68) Peebles, L. R.; Marshall, P. High-Accuracy Coupled-Cluster Computations of Bond Dissociation Energies in SH, H_2S, and H_2O. *J. Chem. Phys.* **2002**, *117*, 3132-3138

(69) Sermiagin, A.; Meyerstein, D.; Bar-Ziv, R.; Zidki, T. The Chemical Properties of Hydrogen Atoms Adsorbed on M^0-Nanoparticles Suspended in Aqueous Solutions: The Case of Ag^0-NPs and Au^0-NPs Reduced by BD_4^-. *Angew. Chem.-Int. Ed*. **2018**, *57*, 16525-16528.

For Table of Contents Only